

Effect of spiral spacing on axial compressive behavior of square reinforced concrete filled steel tube (RCFST) columns

Qiyun Qiao¹, Wenwen Zhang¹, Ben Mou^{*2} and Wanlin Cao¹

¹ College of Architecture and Civil Engineering, Beijing University of Technology, Beijing, 100124, P.R. China

² School of Civil Engineering, Qingdao University of Technology, Qingdao, 266033, P.R. China

(Received June 8, 2018, Revised January 25, 2019, Accepted May 10, 2019)

Abstract. Spiral spacing effect on axial compressive behavior of reinforced concrete filled steel tube (RCFST) stub column is experimentally investigated in this paper. A total of twenty specimens including sixteen square RCFST columns and four benchmarked conventional square concrete filled steel tube (CFST) columns are fabricated and tested. Test variables include spiral spacing (spiral ratio) and concrete strength. The failure modes, load versus displacement curves, compressive rigidity, axial compressive strength, and ductility of the specimens are obtained and analyzed. Especially, the effect of spiral spacing on axial compressive strength and ductility is investigated and discussed in detail. Test results show that heavily arranged spirals considerably increase the ultimate compressive strength but lightly arranged spirals have no obvious effect on the ultimate strength. In practical design, the effect of spirals on RCFST column strength should be considered only when spirals are heavily arranged. Spiral spacing has a considerable effect on increasing the post-peak ductility of RCFST columns. Decreasing of the spiral spacing considerably increases the post-peak ductility of the RCFSTs. When the concrete strength increases, ultimate strength increases but the ductility decreases, due to the brittleness of the higher strength concrete. Arranging spirals, even with a rather small amount of spirals, is an economical and easy solution for improving the ductility of RCFST columns with high-strength concrete. Ultimate compressive strengths of the columns are calculated according to the codes EC4 (2004), GB 50936 (2014), AIJ (2008), and ACI 318 (2014). The ultimate strength of RCFST stub columns can be most precisely evaluated using standard GB 50936 (2014) considering the effect of spiral confinement on core concrete.

Keywords: RCFST; spiral spacing; axial compression; ultimate strength; ductility

1. Introduction

Concrete filled steel tube (CFST) structures are widely used in buildings and bridges, due to the excellent constructional efficiency and mechanical behavior of CFSTs (Qu *et al.* 2015, Pons *et al.* 2018, Ritchie *et al.* 2018, Mou *et al.* 2018, Qiao *et al.* 2019). Two commonly used sections of CFST columns are circular and square sections. Square CFST columns are commonly used due to easy construction and architectural design considerations. However, compared to circular steel tube, square steel tube provides a lower confinement to the concrete; in consequence, the compressive strength and ductility are lower for the square CFST.

There are numerous methods for improving the behavior of square CFST columns, such as: (1) welding stiffeners onto the steel tube (Lee *et al.* 2017); (2) arranging the binding bars (Liu and Cai 2013); (3) inserting an additional steel tube (Hassan *et al.* 2016). Apart from these methods, insertion of longitudinal reinforcing bars into CFST columns (Fig. 1), commonly defined as reinforced concrete filled steel tube (RCFST) columns, are increasingly used in the construction. In many high-rise buildings, such as the

Shin-Osaka Hankyu (80 meters, Japan) and Nakano central park (99 meters, Japan), RCFST structures are used. Numerous studies have already been carried out on the mechanical behavior of the RCFST columns. Xiamuxi and Hasegawa (2012) carried out compression tests on RCFST columns with different axial reinforcement ratios. Results showed that proper reinforcement ratio can improve the overall performance of RCFSTs. Krishan *et al.* (2017) presented a numerical analysis on the ultimate strength of RCFST stub columns and recommended to use high-strength longitudinal reinforcement for further increase of the efficiency of RCFST columns. Moon *et al.* (2013) undertook an analytical research study to evaluate and improve design provisions for CFSTs with and without internal reinforcement under combined axial load and bending and proposed an alternative *P-M* interaction curve for CFSTs. Wei *et al.* (2014) carried out compression tests on RCFSTs to study the effect of concrete strength and steel tube width-to-thickness ratio.

In the design of RCFST structure, transverse reinforcements are commonly arranged around the longitudinal bars (AIJ 2008). These transverse reinforcements can provide an additional confinement to the enclosed concrete and improve the strength and ductility of the columns. The effect of the transverse reinforcement on the mechanical behavior of reinforced concrete (RC) columns has already been extensively studied in the past decades. Hoops or

*Corresponding author, Lecturer,
E-mail: mouben@qut.edu.cn

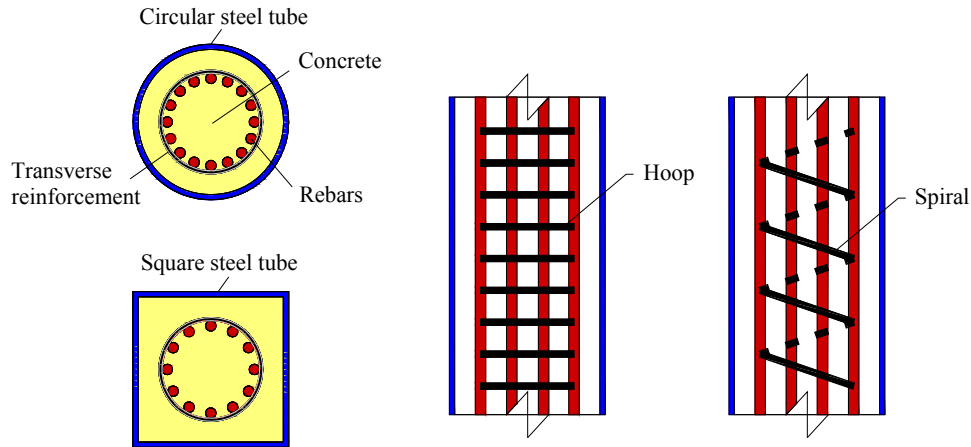


Fig. 1 Schematic diagram of RCFST columns

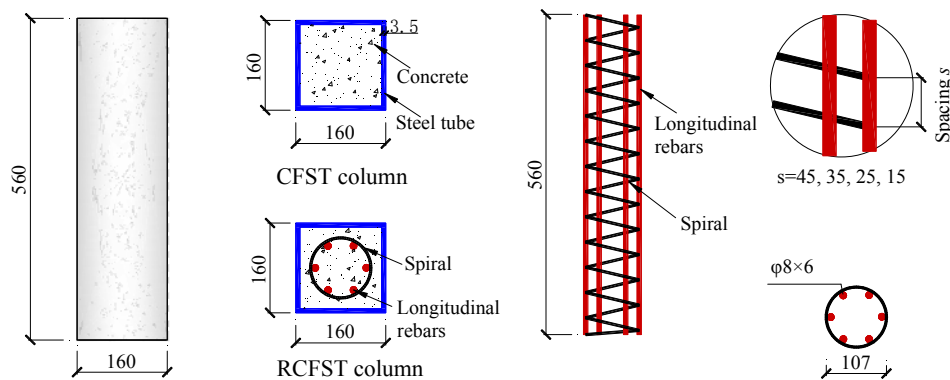


Fig. 2 Details and dimensions of the specimens (Unit: mm)

spirals are the common forms of the transverse reinforcements. Both hoops and spirals can enhance the compressive strength and ductility of RCs, but spirals are much more effective than hoops, because spirals can provide a higher confinement to the enclosed concrete than the hoops. In addition, the ductility, rather than the strength, is the most significant mechanical difference between RC columns with hoops and spirals (Nilson *et al.* 2009). Furthermore, spiral spacing was confirmed to play an important role in the axial compressive behavior of the spiral RC columns (Marvel *et al.* 2014).

Although there are numerous studies on RC columns, investigations into the transverse reinforcement's effect on RCFST columns are rather limited. Ding *et al.* (2016) carried out a series of studies on the compressive behavior of the innovative stirrup-confined CFST stub columns, in which the stirrups were welded onto the steel tube. Hamidian *et al.* (2016) investigated the axial compressive behavior of the circular RCFST columns with different spiral spacings, and confirmed that the spiral spacing has a significant effect on post-peak behavior of the circular columns. So far, no studies on effect of the spiral spacing on the compressive behavior of square RCFST column exist, despite its increasing applications in the engineering practice.

This paper focuses on the compressive behavior of square RCFST columns with different spiral spacings and

concrete strengths. The effect of spiral spacing on ultimate compressive strength and ductility of the RCFST columns is investigated and discussed in detail. The axial compressive strength of the specimens is calculated according to the codes EC4 (2004), GB 50936 (2014), AIJ (2008), and ACI 318 (2014). Design recommendations based on the test results are given to provide references for practical engineering.

2. Experimental investigation

2.1 Test specimens

A total of twenty reduced-scale specimens, including sixteen RCFST columns with spirals and four benchmarked conventional CFST columns without spirals, were designed and fabricated. Based on the concrete strength, the specimens were divided into two groups, namely group 1 and group 2. Group 1 included ten columns with normal-strength concrete, and group 2 included ten columns with high-strength concrete. Fig. 2 and Table 1 show the detailed configuration of the specimens. The nominal width (B) and wall thickness (t) of the steel tube were 160 mm and 3.5 mm, respectively. The measured values of B and t are shown in Table 1. The B/t ratio of the steel tube was 46. According to the AISC360-16, the steel tube is classified as

Table 1 Specimens details

Specimen ID	B (mm)	t (mm)	H (mm)	D_l (mm)	n	d_s (mm)	s (mm)	ρ_{sp} (%)	f_c' (N/mm ²)	λ_{sp} (%)
N-CFST-1 N-CFST-2	159.31	3.47	560	8	6	4	0	0	37.2	0.00
N-45-1 N-45-2	159.31	3.47	560	8	6	4	45	1.14	37.2	8.20
N-35-1 N-35-2	159.31	3.47	560	8	6	4	35	1.46	37.2	10.55
N-25-1 N-25-2	159.31	3.47	560	8	6	4	25	2.03	37.2	14.76
N-15-1 N-15-2	159.31	3.47	560	8	6	4	15	3.38	37.2	24.61
H-CFST-1 H-CFST-2	159.27	3.49	560	8	6	4	0	0	50.3	0.00
H-45-1 H-45-2	159.27	3.49	560	8	6	4	45	1.14	50.3	6.07
H-35-1 H-35-2	159.27	3.49	560	8	6	4	35	1.46	50.3	7.80
H-25-1 H-25-2	159.27	3.49	560	8	6	4	25	2.03	50.3	10.93
H-15-1 H-15-2	159.27	3.49	560	8	6	4	15	3.38	50.3	18.21

*Note: B is the width of the steel tube; t is the wall thickness of the steel tube; H is the height of the specimen; D_l and n are the diameter and number of the rebars, respectively; d_s , s , and ρ_{sp} are the diameter, spacing and volumetric ratio of the spirals, respectively; f_c' is the cylinder compressive strength of the concrete; λ_{sp} is the spiral confinement effect

compact section. All the columns were 560 mm tall, with the height-width ratio (H/B) of 3.5, thus the columns were considered as the stub columns (AIJ 2008). For each group, five different conditions were designed, which were the spirally-confined RCFST columns with four different spiral

spacings and conventional CFST column without spirals. Two identical specimens were conducted for each condition to ensure the reliability of the test results and reduce error. The diameter of the spirally-confined core concrete, measured from center to center of the perimeter spiral, was



(a) Spiral spacing



(b) Spirals



(c) Square steel tubes

Fig. 3 Photographs showing the spirals and steel tubes

Table 2 Properties of concrete

Concrete	f_{cu}^{150} (N/mm ²)	f_c' (N/mm ²)	E_c (N/mm ²)
Normal-strength	48.9	37.2	3.14×10^4
High-strength	63.9	50.3	3.37×10^4

107 mm. The diameter of the spiral was 4 mm, and spiral spacings were 45 mm, 35 mm, 25 mm, and 15 mm. The corresponding volumetric-spiral ratios ρ_{sp} were 1.14%, 1.46%, 2.03%, and 3.38%, respectively. Here, ρ_{sp} is defined as the spiral volume (V_{sp}) divided by the core concrete volume confined by the spiral (V_{sc}).

In the RCFST columns, six longitudinal reinforcing bars with 8 mm diameter were used to form the reinforcement cage. In ACI 318 (2014) or GB 50010 (2010), six is the minimum number of longitudinal bars in the circular RC columns. The ratio of the longitudinal bars area to the gross area of the column was 0.012, which was near the lower limit of 0.01 required in ACI 318 (2014).

Fig. 3 shows the preparations of the specimens. Firstly, the steel tubes were cut and machined to the required height. Then, spiral reinforcement cages with different spiral spacing were manufactured and installed into the steel tubes concentrically. After that, the concrete was poured from the top of the specimens and vibrated carefully. All the specimens were cured at room temperature. Meanwhile, standard concrete cube and prism specimens were prepared and cured in the same condition. After a certain period of curing, because of the concrete shrinkage, the concrete surface was slightly lower than that of the steel tube. Thus, high strength grout was used to smooth the surface of the columns before the test.

Specimen N-45-1 is used as an example to explain the labeling scheme of the specimens in Table 1. (1) “N” refers to the normal-strength concrete, while H refers to the high-strength concrete; (2) “45” refers to spiral spacing $s=45$ mm, while 35, 25 and 15 refer to the spiral spacing $s=35$, 25, and 15 mm, respectively; (3) “1” refers to the first specimen of the two identical specimens, while 2 refers to

Table 3 Mechanical properties of steel materials

Steel material	d or t (mm)	f_y (N/mm ²)	f_u (N/mm ²)	E_s (N/mm ²)	δ (%)
Steel tube	3.5	359	478	1.89×10^5	27.2
Longitudinal re-bar	8.0	474	690	1.93×10^5	26.8
Spiral	4.0	280	349	1.58×10^5	27.5

*Note: d is the diameter, t is the wall thickness; f_y , f_u , E_s , and δ are the yield strength, ultimate strength, Young’s modulus and elongation, respectively

the second specimen. Note that N-CFST and H-CFST refer to the conventional CFST columns with normal-strength concrete and high-strength concrete, respectively.

2.2 Material properties

Three concrete cube specimens with $150 \times 150 \times 150$ mm dimensions for each concrete grade were casted and tested on the basis of GB/T 50081 (2002). The mean cube strengths f_{cu}^{150} of normal and high strength concrete were 48.9 N/mm² and 63.9 N/mm² at the day of the test, respectively. Note that cube strength, rather than the cylinder strength, is used for determining concrete compressive strength in China. For convenience of analysis, the concrete cube strength was converted to the cylinder strength (GB 50010 2010). The converted cylinder strength f_c' of normal-strength concrete and high-strength concrete were 37.2 N/mm² and 50.3 N/mm², respectively. Three concrete prism specimens $150 \times 150 \times 300$ mm in size for each concrete grade were casted and tested according to the standard GB/T 50081 (2002) to obtain Young’s modulus E_c . Properties of the concrete are shown in Table 2.

Steel tube material properties were obtained from tensile tests of coupons taken from the middle of the steel tube. Three tensile tests were conducted for each type of the steel. The yield strength f_y , ultimate strength f_u , Young’s modulus E_s , and elongation δ for the steel tubes, longitudinal reinforcing bars, and spirals are shown in Table 3.

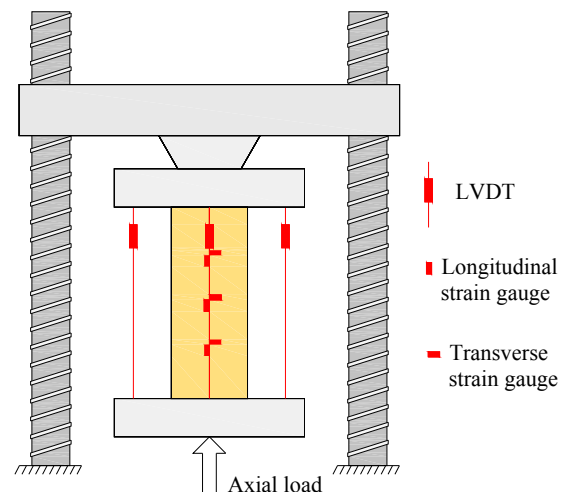


Fig. 4 Test setup

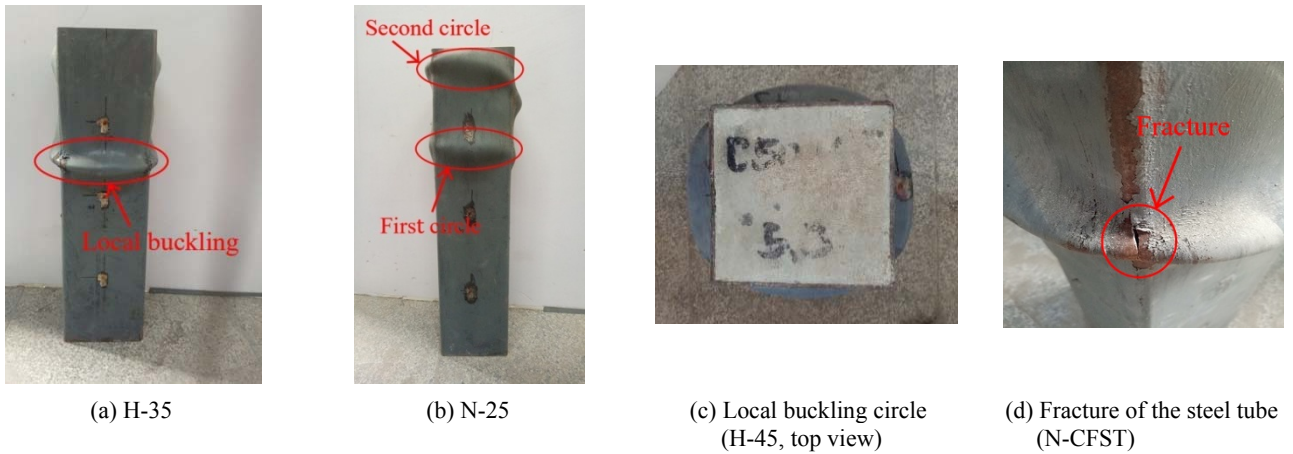


Fig. 5 Photographs showing failure modes of typical specimens

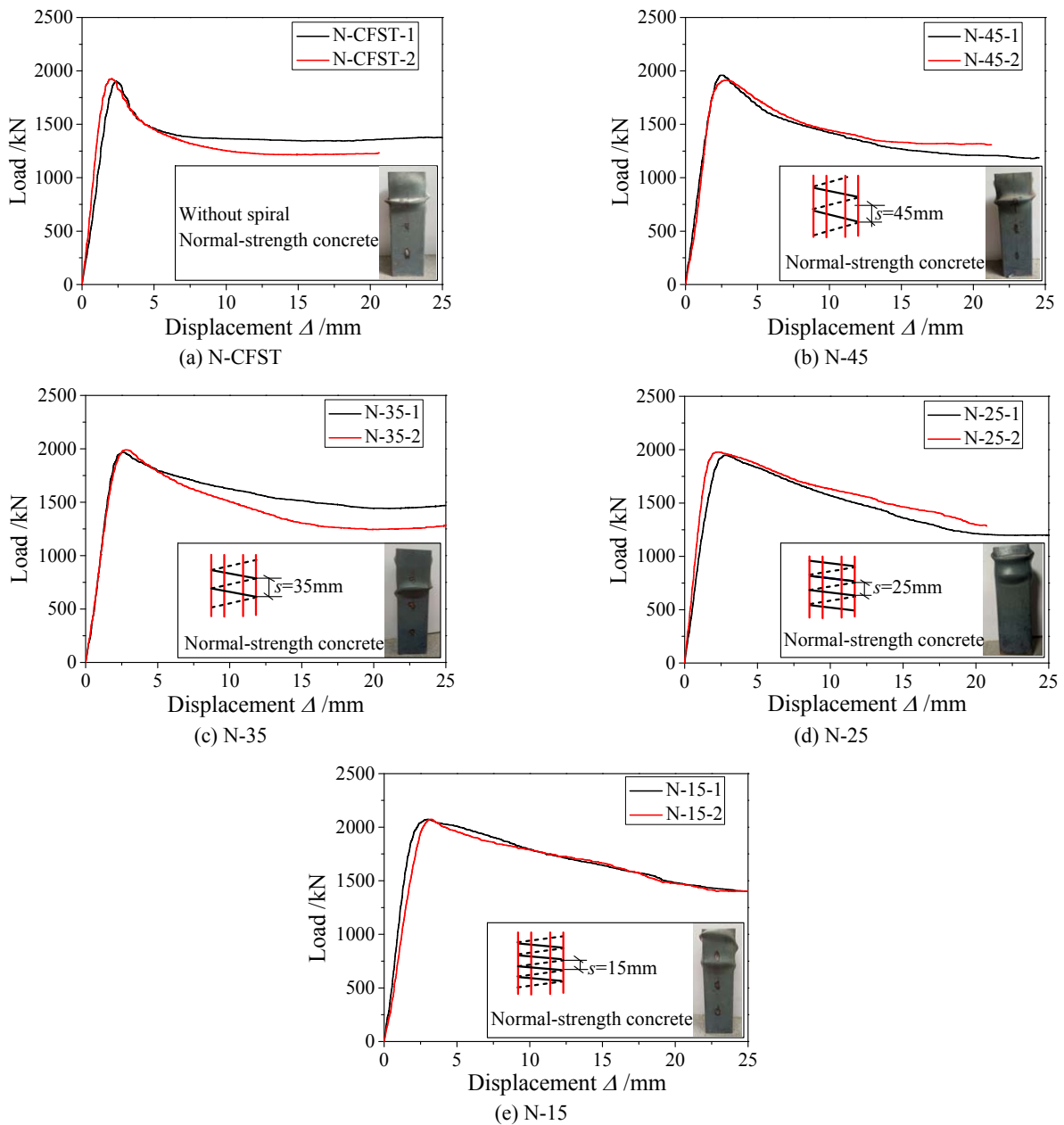


Fig. 6 Load versus displacement curves for normal-strength concrete specimens

2.3 Test setup and measurements

Axial compressive tests were conducted using a 3000 kN capacity testing machine in the structural laboratory at Beijing university of technology, as shown in Fig. 4. An axial compressive load was applied to the specimen in a monotonic manner with a loading rate of 1 mm/min until the end of the test. Four linear variable displacement transducers (LVDTs) were installed on each side of specimen to measure the axial displacement. Bi-directional strain gauges were mounted on the steel tube to measure longitudinal and transverse strain, as shown in Fig. 4.

3. Test results

3.1 Failure modes

Figs. 5(a)-(b) show the photographs of the typical specimens H-35 and N-25 at failure. All the specimens show similar final failure modes in a rather ductile manner. In the early loading stage, no obvious changes are observed in the specimens' appearance. When the load reaches to 80%-90% of the peak load in the pre-peak stage, a slight local buckling at one side of the steel tube can be found. At the peak load, the damage mode for all RCFST columns is

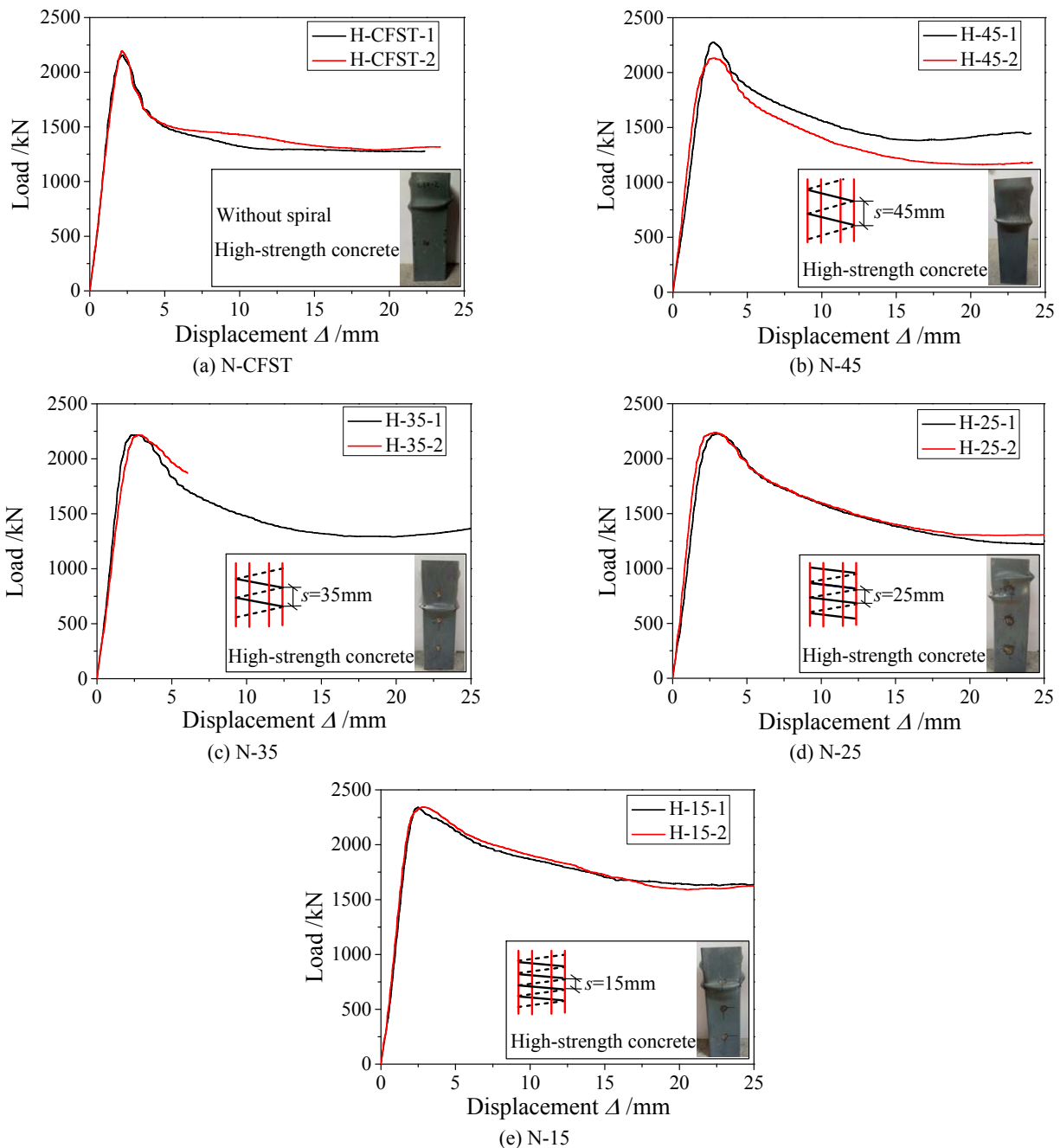


Fig. 7 Load versus displacement curves for high-strength concrete specimens

the obvious visible outward local buckling. After the peak load, the strength drops rapidly, accompany with the development of the local buckling. When the load drops to 70%-80% of the peak load, the local buckling circle is formed as shown in Fig. 5(c). After that, with increasing the axial displacement, some of the specimens exhibit the second local buckling circle, as shown in Fig. 5(b). Also, some of the steel tubes fractured at the corners, as shown in Fig. 5(d).

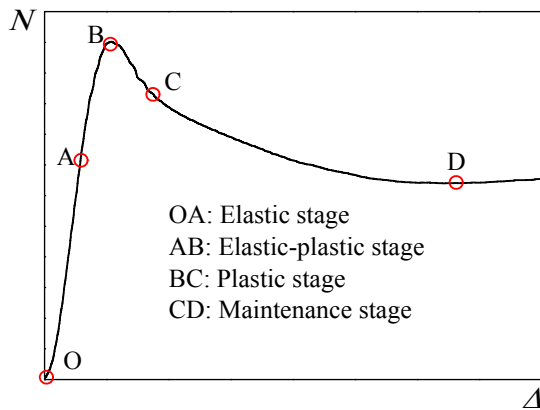
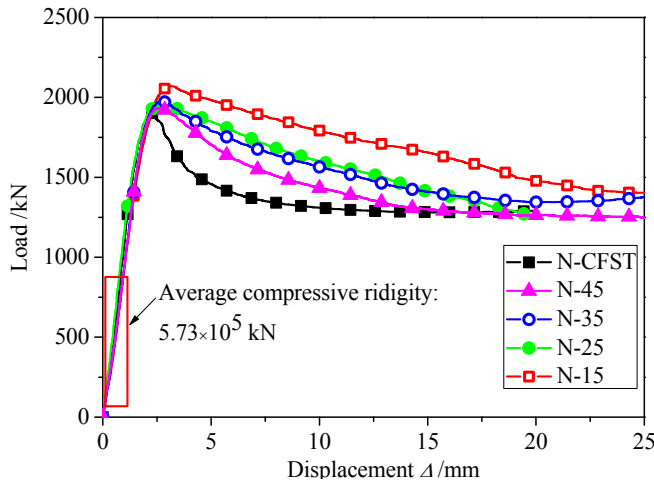


Fig. 8 Graph showing a typical axial load versus axial deformation relationship

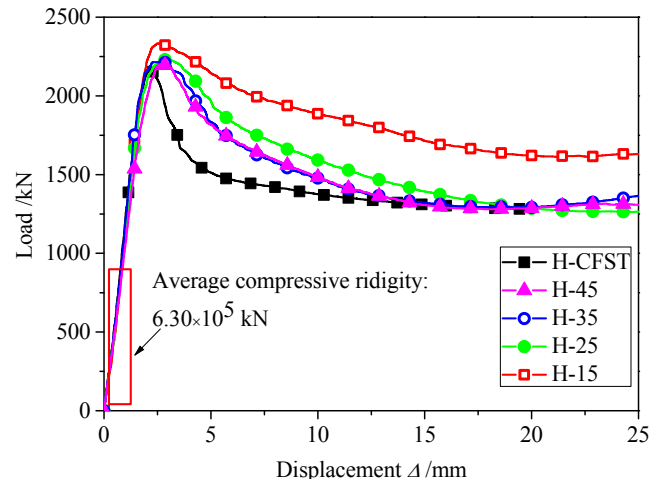
3.2 Load versus displacement curves

Figs. 6-7 show the load versus axial displacement relationships for the normal-strength and high-strength concrete specimens, respectively. Fig. 8 shows the schematic view of a typical load versus displacement relationship of the specimens, which can be generally divided into four stages: (1) Elastic stage (OA). The columns behave in an elastic manner and it is commonly considered that there is no interaction between the steel tube and concrete. (2) Elastic-plastic stage (AB). Point B refers to the peak load, which is defined as the ultimate strength of the columns. (3) Plastic stage (BC). Point C refers to the point when the load decreases to 85% of the peak load. Load decreases rapidly in this stage due to the concrete crushing and local buckling. (4) Maintenance stage (CD). Point D refers to the point when the load reaches the minimum. In this stage, the rate of load decrease slows down.

Fig. 9 compares the load versus deformation relationships for specimens with different spiral spacings. In the pre-peak stage, the curves are similar. There are no obvious differences between the ultimate strengths of specimens with spiral spacing of 45, 35, and 25 mm; however, for specimens with a spiral spacing of 15 mm, the ultimate strength increases considerably compared with other RCFST specimens. This is because when the spirals are heavily arranged, confinement to the core concrete



(a) Normal-strength concrete specimens



(b) High-strength concrete specimens

Fig. 9 Mean curves of load-displacement for specimens with different spiral spacing

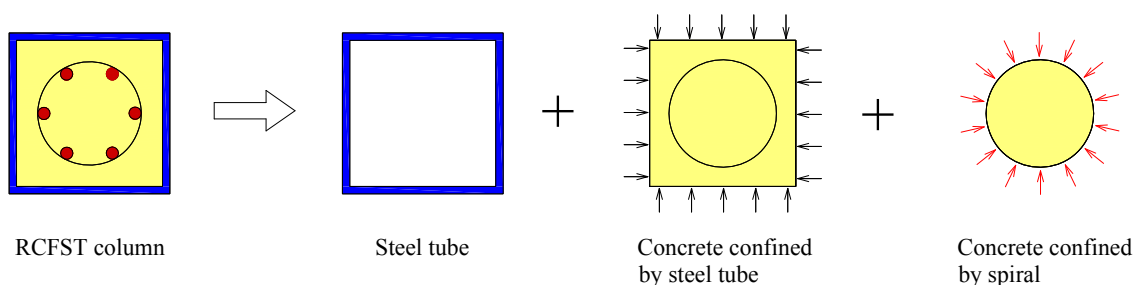


Fig. 10 Schematic diagram showing the dual confinement mechanism

provided by the spirals is relatively high, thus the compressive strength of the concrete increases considerably. In the post-peak stage, the curves are quite different depending on the spiral spacings. Strength of the conventional CFST specimen drops sharply after the peak load, however, the RCFST specimens exhibit a slower descending branch due to the inserted reinforcement cages. In addition, with decreasing the spiral spacing, the specimens exhibit a less steep descending branch. Decreasing of the spiral spacing enhances the transverse confinement of the core concrete, which slows down the crack development, resulting in increased ductility after the peak load. Fig. 10 shows the mechanism of the dual confinement provided by both square steel tube and spirals. In Fig. 10, the concrete confined by the steel tube is the square section with dimension of 153×153 mm; the core concrete additionally confined by the spiral is the circular section with diameter of 103 mm.

4. Analysis and discussions

4.1 Rigidity

Compressive rigidity ($E_{sc}A_{sc}$) is defined as the secant stiffness when strength is equal to 40% of the ultimate strength (Huo *et al.* 2009). It is calculated as follows

$$E_{sc}A_{sc} = \frac{0.4N_u}{\varepsilon_{0.4}} = \frac{0.4N_u}{A_{0.4}/H} \quad (1)$$

Where, N_u is the ultimate strength; $\varepsilon_{0.4}$ and $A_{0.4}$ is the compressive strain and displacement corresponding to $0.4N_u$, respectively; H is the height of the columns.

The elastic stage of the load versus displacement curves in Fig. 9 show almost no differences, indicating that the spiral spacing has almost no effect on compressive rigidity. Similar results were also exhibited in the studies of RC columns by Marvel *et al.* (2014). The average compressive rigidity of high-strength concrete specimens (i.e., 6.30×10^5 kN) is 9.95% higher than that of normal-strength concrete specimens (i.e., 5.73×10^5 kN), this is because the concrete modulus of elasticity E_c increases with increasing the concrete strength.

4.2 Strength

For convenience of discussions, a strength index (SI) is defined to evaluate the compressive ultimate strength as follows (Han *et al.* 2010)

$$SI = N_{u,RCFST} / N_{u,CFST} \quad (2)$$

Where, $N_{u,RCFST}$ is the measured ultimate compressive strength of RCFST column, and $N_{u,CFST}$ is the ultimate strength of the benchmarked conventional CFST column.

Fig. 11 shows the SI of all the specimens. Based on Fig. 11, the effects of the spiral spacing and concrete strength on the SI are discussed as follows.

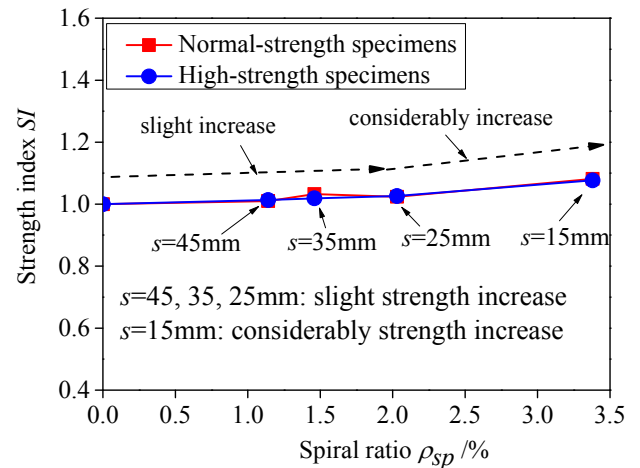


Fig. 11 Effect of the spiral ratio ρ_{sp} on strength index (SI)

4.2.1 Spiral spacing

The strengths of the RCFST columns are higher than those of conventional CFST columns, because the longitudinal reinforcing bars and spirals enhance the ultimate strength of the columns. More specifically, the SI is 1.01, 1.03, 1.02, and 1.08 for normal-strength specimens N-45, N-35, N-25, and N-15, respectively; while for high-strength specimens H-45, H-35, H-25, and H-15, the SI is 1.01, 1.02, 1.03, and 1.08, respectively. There is a trend that decreasing the spiral spacing resulted in the increase of the ultimate strength. When decreasing the spiral spacing, the spiral ratio increases. In consequence, the confinement provided by the spirals increases, which results in the slower growth of the lateral expansion of the core concrete confined by the spirals. Thus, the local buckling of the steel tube could be restrained by the application of spiral confinements. Similar results were also obtained by Ding *et al.* (2016). In addition, for spiral spacing of 45, 35 and 25 mm, the strength increase is slight; however, for spiral spacing of 15 mm, the strength is considerably increased. For a spirally-confined RC short column under axial compression, the existence of the spirals would increase the ultimate compressive strength of the RC column, depending on the spiral spacing. When the spiral spacing is large, there is little increase in the compressive strength. However, when the spiral spacing is small, the increase of the compressive strength is considerable. In the GB 50010 (2010), it defines such a critical spiral spacing s for a spirally-confined RC column, which reads

$$s \leq \min \{80 \text{ mm}, D_{sc} / 5\} \quad (3)$$

Where D_{sc} is the diameter of core concrete confined by the spirals.

In this study, it is found that the above phenomenon also applies for the RCFST column. It is suggested that the Eq. (3) can be used to define the critical spiral spacing for a spirally-confined RCFST column as well.

4.2.2 Concrete strength

Concrete strength is an important parameter affecting

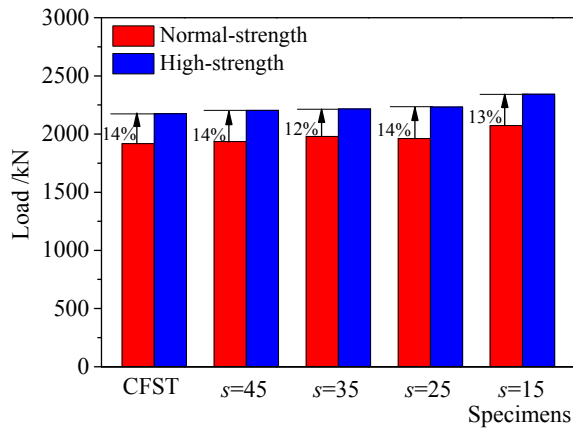


Fig. 12 Effect of the concrete strength on the ultimate strength

the compressive strength of columns. Fig. 12 shows the effect of the concrete strength on the ultimate strength. It is easily seen graphically that the ultimate strength increases with increasing the concrete strength. For high-strength concrete specimens, the ultimate bearing capacity increases by 14% on average, due to the increased strength contribution from the higher strength concrete.

4.3 Ductility

In order to investigate the effect of spiral spacing on the ductility of RCFST stub columns, a ductility index (DI) (Han 2002), is defined as

$$DI = \Delta_{0.85} / \Delta_b \quad (4)$$

Where $\Delta_{0.85}$ is the axial displacement when strength drops to 85% of the ultimate strength, Δ_b is equal to $\Delta_{0.75}/0.75$, $\Delta_{0.75}$ is the corresponding axial displacement when strength equals to 75% of the ultimate strength in the pre-peak stage.

Table 4 summaries the $\Delta_{0.85}$, Δ_b and the ductility index (DI). Here, DI values are the average values of the two identical specimens. A larger value of DI refers to slower

strength degradation after the peak load, corresponding to a higher ductility. The effects of the spiral spacing and concrete strength on the DI are discussed as follows.

4.3.1 Spiral spacing

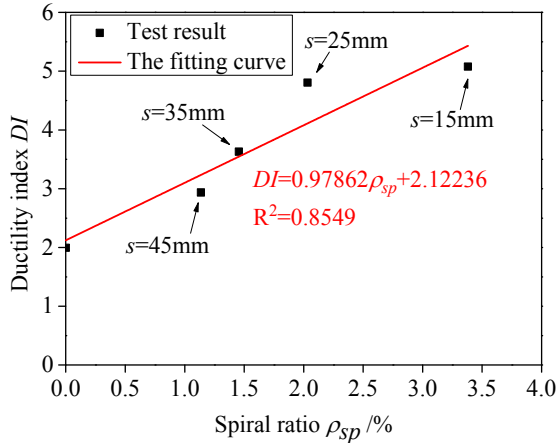
Fig. 13 gives the relationship between DI and spiral ratio ρ_{sp} (spiral spacing), in which a linear relationship between DI and spiral ratio is confirmed. DI values of normal-strength concrete specimens N-45, N-35, N-25, and N-15 are 47%, 82%, 141%, and 154% larger than that of specimen N-CFST, respectively; as for high-strength concrete specimens H-45, H-35, H-25, and H-15, DI values are improved by 31%, 60%, 64%, and 116%, respectively. For all the specimens, DI values, on average, improved by 39%, 72%, 103%, and 135% for specimens with $s = 45, 35, 25$ and 15 mm, respectively. These increases clearly demonstrate that spiral ratio (spiral spacing) plays a significant role in RCFST columns ductility.

4.3.2 Concrete strength

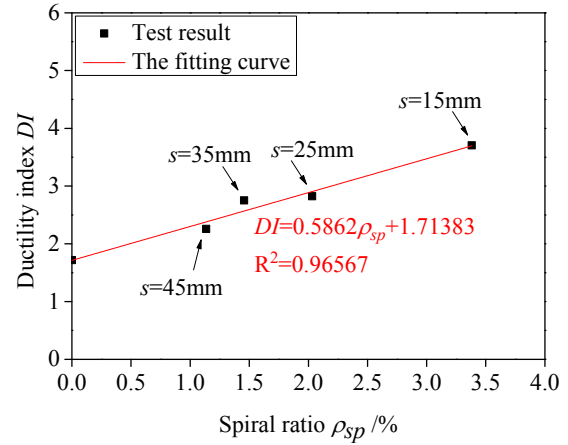
Fig. 14 shows the comparison of ductility for normal-strength concrete and high-strength concrete specimens. It is indicated that when concrete strength increases, the DI decreases considerably due to the brittleness of the higher strength concrete. In the CFST column design, high-strength concrete tends to be used to improve column strength and minimize column cross-section area. However, the strength increase comes at a cost in a decrease of ductility due to the higher strength concrete; in consequence, the ductility of CFST column with high-strength concrete is always a concern in engineering practice. Increasing the thickness of the steel tube is a method to solve the ductility issue of the CFST column with high-strength concrete, but it may not be economical (Hamidian *et al.* 2016). When comparing high-strength concrete specimen H-45 and normal-strength concrete specimen N-CFST, the DI of H-45 (i.e., 2.26) is 13.0% higher than that of N-CFST (i.e., 2.00), indicating that spirals in high-strength concrete results in a better ductility compared to normal-strength CFST without spirals. It should be noted that for specimen H-45, the spiral ratio is 1.14%, which is much lower than the requirements of the spirally-confined RC columns in ACI 318 (2014). Thus

Table 4 Ductility of specimens

Group	Specimen ID	Spacing (mm)	ρ_{sp} (%)	$\Delta_{0.75}$	Δ_b	$\Delta_{0.85}$	DI
Group 1	N-CFST	-	0	1.33	1.77	3.46	2.00
	N-45	45	1.14	1.47	1.96	5.74	2.94
	N-35	35	1.46	1.52	2.02	7.31	3.63
	N-25	25	2.03	1.33	1.77	8.34	4.81
	N-15	15	3.38	1.65	2.20	10.93	5.08
Group 2	H-CFST	-	0	1.34	1.79	3.08	1.72
	H-45	45	1.14	1.53	2.04	4.55	2.26
	H-35	35	1.46	1.46	1.94	5.35	2.75
	H-25	25	2.03	1.45	1.93	5.40	2.83
	H-15	15	3.38	1.48	1.97	7.26	3.71



(a) Normal-strength concrete specimens



(b) High-strength concrete specimens

Fig. 13 Ductility index DI versus spiral ratio ρ_{sp} relationships

arranging the spirals, even with a small spiral ratio, is an economical and easy solution for solving the ductility issue, expanding the application of high-strength concrete in the CFST columns.

4.4 Spiral confinement effect

The confinement provided by the spiral is different for normal strength and high strength concrete. Thus, a parameter named spiral confinement effect λ_{sp} including the effect of concrete strength and spiral ratio is calculated as follows

$$\lambda_{sp} = \rho_{sp} \frac{f_{yv}}{f_c} \tag{5}$$

Where, ρ_{sp} is the volumetric-spiral ratio; f_{yv} is the yield strength of the spiral; f_c is the concrete cylinder strength.

The calculated spiral confinement effect λ_{sp} is listed in Table 1. Figs. 15(a) and (b) show the strength index (SI) versus λ_{sp} relationships and relative ductility index (RDI) versus λ_{sp} relationships, respectively. Here, the RDI is the DI of the RCFST specimens divided by the DI of the CFST specimens (i.e., $RDI = DI_{RCFST}/DI_{CFST}$). There is a trend that the strength and ductility increases with increasing the spiral confinement effect λ_{sp} . This is because the greater λ_{sp} value indicates a higher confinement provided by the spiral to the core concrete.

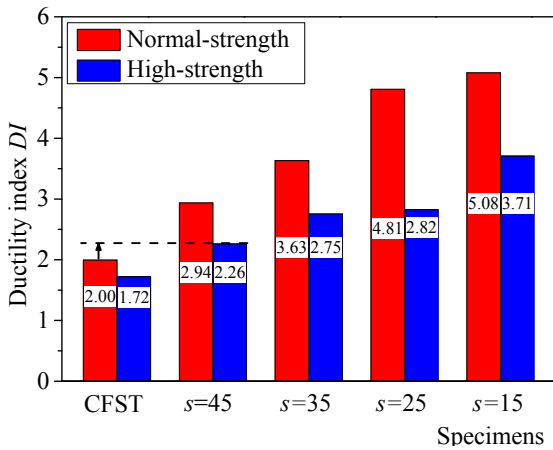
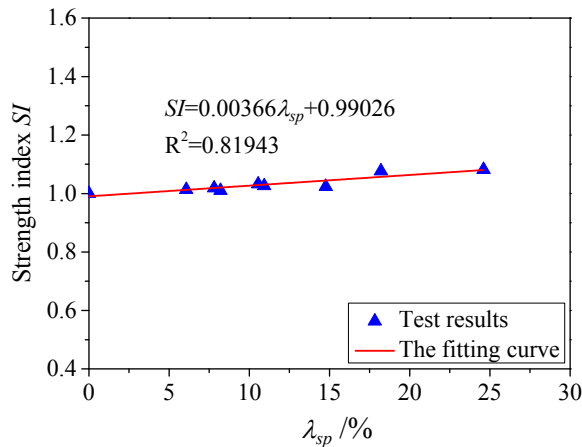
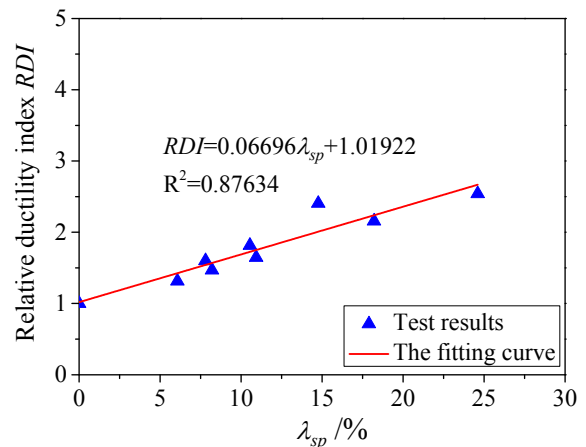


Fig. 14 Comparison of ductility for normal-strength and high-strength specimens



(a) SI versus λ_{sp} relationships



(b) RDI versus λ_{sp} relationships

Fig. 15 Effect of λ_{sp} on strength and ductility

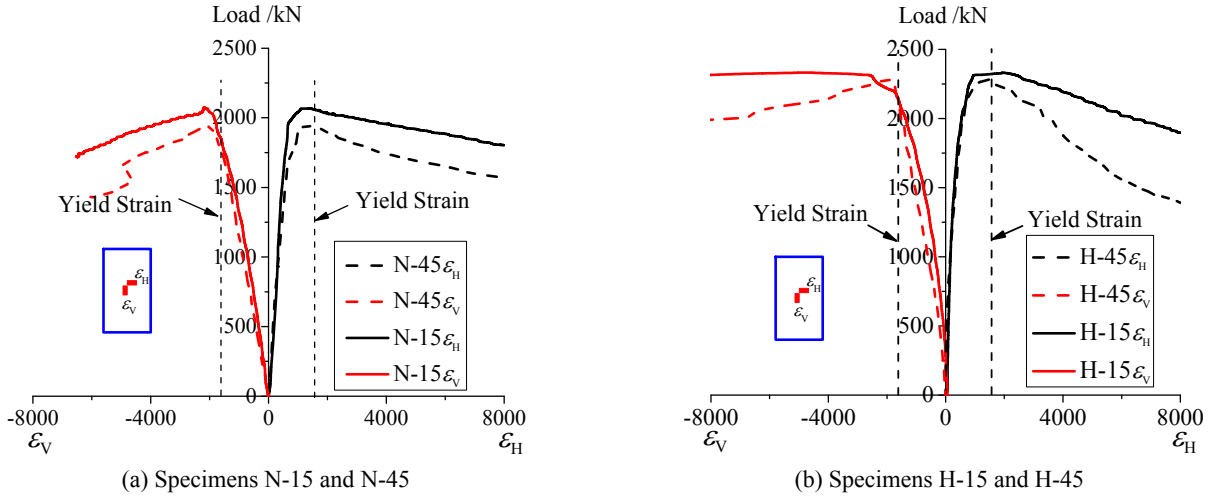


Fig. 16 Load versus strain curves of steel tubes

4.5 Strain Analysis

Fig. 16 shows the load versus strain curves of the typical specimens with $s = 15$ and 45 mm. In Fig. 16, ε_H is the measured hoop strain of the steel tube, and ε_V is the measured longitudinal strain of the steel tube. There are no obvious differences in the trend of load versus strain curves for different specimens. The load versus strain response is nearly linear in the early loading stage. As loading increases to approximately 80% of the ultimate strength, the curves present an inelastic response. Longitudinal strain reaches the yield strain before the ultimate strength, while the hoop strain reaches the yield strain near the ultimate strength.

4.6 Design suggestions

Axial compressive strengths of the specimens are calculated according to the codes EC4 (2004), GB 50936 (2014), AIJ (2008), and ACI 318 (2014). The effects of the steel tube, concrete, and longitudinal reinforcing bars are considered when evaluating the ultimate compressive strength.

In the evaluation of ultimate strength, according to the aforementioned requirements on the spiral spacing in Eq. (3), the strength increase is considered only for the specimens with spiral spacing of 15 mm. The concrete axial compressive strength confined by the spirals is calculated based on Eq. (6), where the yield strength is used for the spirals (GB50010).

$$f'_{cc} = f'_c + 4f_r \quad (6a)$$

$$f_r = \frac{2A_{ss,1}f_{yv}}{D_{sc}s} \quad (6b)$$

Where, f'_{cc} is the axial compressive strength of concrete confined by the spiral; f'_c is the concrete cylinder strength; f_r is the lateral pressure of the spiral on its confined concrete, which is calculated based on the equilibrium of forces, as shown in Fig. 17; $A_{ss,1}$ is the cross-section area of spiral; f_{yv}

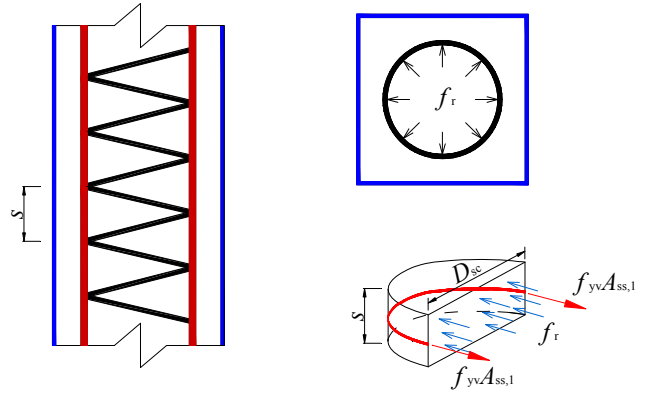


Fig. 17 Confining stress provided by the spiral

is the yield strength of spiral. D_{sc} is the diameter of core concrete confined by the spirals.

4.6.1 EC4

EC4 presents a formula for predicting axial compressive strength of the CFST with longitudinal reinforcing bars

$$N_{EC4} = \eta_a A_{st} f_{yt} + A_c f'_c \left(1 + \eta_c \frac{t f_{yt}}{b f'_c}\right) + A_{sb} f_{yb} \quad (7)$$

Where, A_{st} is the cross-section area of steel tube; f_{yt} is the yield strength of steel tube; A_c is the cross-section area of concrete; f'_c is the concrete cylinder strength; t is the thickness of steel tube; b is the width of concrete enclosed by steel tube; A_{sb} is the cross-section area of longitudinal reinforcing bars; f_{yb} is the yield strength of longitudinal reinforcing bar.

The values $\eta_a = \eta_{a0}$ and $\eta_c = \eta_{c0}$ are given by Eqs. (7a)-(7b), respectively

$$\eta_{a0} = 0.25(3 + 2\bar{\lambda}) \quad (8a)$$

$$\eta_{c0} = 4.9 - 18.5\bar{\lambda} + 17\bar{\lambda}^2 \quad (8b)$$

$$\bar{\lambda} = \sqrt{\frac{N_{pl,Rk}}{N_{cr}}} \quad (8c)$$

$$N_{pl,Rk} = A_{st} \frac{f_{yt}}{\gamma_{Ma}} + A_c \frac{f'_c}{\gamma_c} + A_{sb} \frac{f_{yb}}{\gamma_s} \quad (8d)$$

$$N_{cr} = \frac{\pi^2 (EI)_{eff}}{l^2} \quad (8e)$$

$$(EI)_{eff} = E_a I_a + E_s I_s + K_e E_c I_c \quad (8f)$$

Where, E_a is the modulus of elasticity of steel tube; E_s is the modulus of elasticity of reinforcing bar; E_c is the secant modulus of elasticity of concrete; I_a is the second moment of area of the steel tube; I_c is the second moment of area of the un-cracked concrete section; I_s is the second moment of area of the reinforcing bar. K_e , γ_{Ma} , γ_c , γ_s are taken as 0.6, 1.1, 1.4, and 1.1, respectively.

4.6.2 GB 50936

In GB 50936, the confinement provided by the square steel to the concrete is considered. The formula is

$$N_{GB} = (1.212 + B \zeta_0 + C \zeta_0^2) (A_{st} + A_c) f'_c + A_{sb} f_{yb} \quad (9)$$

Where

$$\zeta_0 = (A_{st} / A_c) \cdot (f_{yt} / f'_c) \quad (10a)$$

$$B = 0.131 \cdot f_{yt} / 213 + 0.723 \quad (10b)$$

$$C = -0.07 \cdot f'_c / 14.4 + 0.026 \quad (10c)$$

4.6.3 AIJ

In the AIJ recommendation for CFST structures, the axial compressive strength of the square CFST column is calculated as the sum of the strength of each component,

which means the interaction between the steel tube and concrete as well as the confinement effect of the square steel tube on the concrete core is not considered. The equation is given as follows

$$N_{AIJ} = A_c f'_c + A_{st} f_{yt} + A_{sb} f_{yb} \quad (11)$$

4.6.4 ACI 318

In ACI 318, when calculating the axial compressive strength of column, the interaction between the steel tube and concrete as well as the confinement effect of the steel tube on the concrete core is not considered. The equation is given as follows

$$N_{ACI} = 0.85 A_c f'_c + A_{st} f_{yt} + A_{sb} f_{yb} \quad (12)$$

4.6.5 Discussions

Table 5 and Fig. 17 show the comparison of the test results and calculated results based on the current codes. On average, the test results are 8% less than predicted results for EC4, 2% less than the predicted results of GB 50936, 9% more than the predicted results of AIJ, and 19% more than the predicted results of ACI 318-14. Results show that the GB 50936 gives the most precise predictions, EC4 gives unsafe predictions, AIJ and ACI predictions are conservative compared to the test results. Table 6 shows predicted contributions of steel tube, concrete, and reinforcing bars to the axial compressive strength according to the four design codes. It is indicated that the steel tube and concrete contribute most of the axial compressive strength.

For EC4, the confinement provided by the square steel tube is considered and the limitation of the B/t ratio is calculated as

$$\frac{B}{t} \leq 52 \sqrt{\frac{235}{f_{yt}}} \quad (13)$$

For GB50936, the confinement provided by the square steel tube is considered and the limitation of the B/t ratio is calculated as

Table 5 Comparisons of the test results and calculated results

Specimen ID	N_{test} (kN)	N_{EC4} (kN)	N_{test}/N_{EC4}	N_{GB} (kN)	N_{test}/N_{GB}	N_{AIJ} (kN)	N_{test}/N_{AIJ}	N_{ACI} (kN)	N_{test}/N_{ACI}
N-CFST	1917	2011	0.95	1847	1.04	1653	1.16	1524	1.26
Group 1	N-45	1936	0.90	1990	0.97	1785	1.08	1657	1.17
	N-35	1979	0.92	1990	0.99	1785	1.11	1657	1.19
	N-25	1962	0.91	1990	0.99	1785	1.10	1657	1.18
	N-15	2073	0.92	2098	0.99	1893	1.10	1765	1.17
	H-CFST	2175	2298	0.95	2202	0.99	1958	1.11	1782
Group 2	H-45	2204	0.90	2345	0.94	2086	1.06	1912	1.15
	H-35	2216	0.91	2345	0.95	2086	1.06	1912	1.16
	H-25	2232	0.91	2345	0.95	2086	1.07	1912	1.17
	H-15	2342	0.92	2443	0.96	2184	1.07	2010	1.17
	Mean			0.92		0.98		1.09	
Sta. Dev.			0.01		0.02		0.02		0.02

Table 6 Contributions of different elements to the axial compressive strength

Specimen ID	N_{EC4}			N_{GB}		N_{AIJ}			N_{ACI}		
	N_{st}	N_c	N_{sb}	$N_{st}+N_c$	N_{sb}	N_{st}	N_c	N_{sb}	N_{st}	N_c	N_{sb}
N-CFST	643	1368	0	1847	143	787	866	0	787	736	0
N-45	643	1368	143	1847	143	787	855	143	787	727	143
N-35	643	1368	143	1847	143	787	855	143	787	727	143
N-25	643	1368	143	1847	143	787	855	143	787	727	143
N-15	643	1476	143	1955	143	787	963	143	787	835	143
H-CFST	646	1652	0	2202	0	787	1171	0	787	995	0
H-45	646	1652	143	2202	143	787	1156	143	787	982	143
H-35	646	1652	143	2202	143	787	1156	143	787	982	143
H-25	646	1652	143	2202	143	787	1156	143	787	982	143
H-15	646	1750	143	2300	143	787	1254	143	787	1080	143

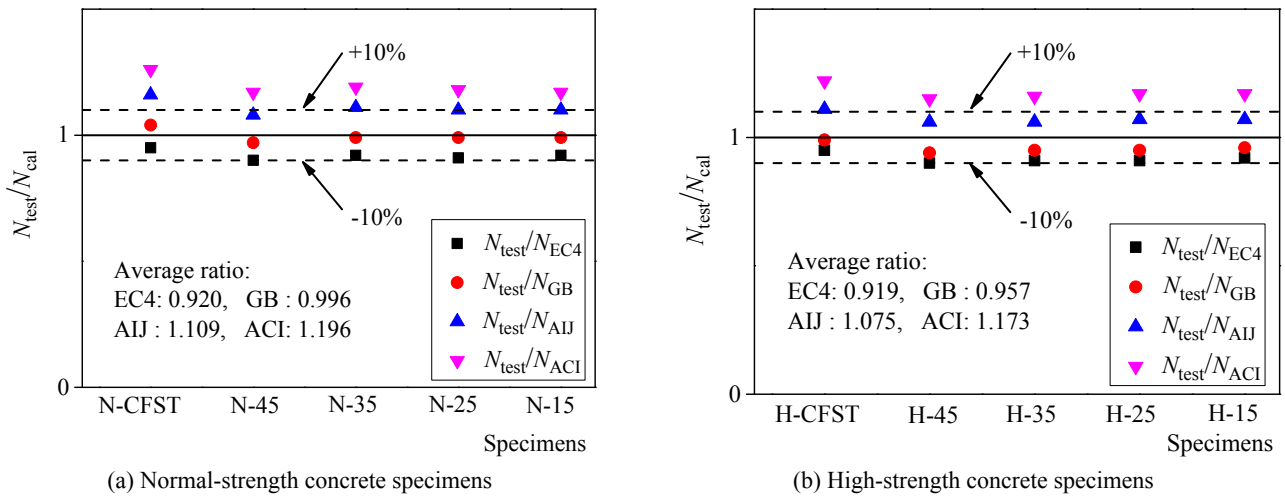


Fig. 18 Comparisons between the test results and calculated results

$$\frac{B}{t} \leq 60 \sqrt{\frac{235}{f_{yt}}} \quad (14)$$

For AIJ, the confinement provided by the square steel tube is not considered and the limitation of the B/t ratio is calculated as

$$\frac{B}{t} \leq 1.5 \frac{23}{\sqrt{f_{yt}/1000}} \quad (15)$$

For ACI318, The confinement provided by the square steel tube is not considered and the limitation of the B/t ratio is calculated as

$$\frac{B}{t} \leq \sqrt{\frac{3E_s}{f_{yt}}} \quad (16)$$

According to the equations above, the limitations of the B/t ratio for EC4, GB50936, AIJ, and ACI318 are 42, 49, 58, and 40, respectively, while the B/t ratio of the test specimens is 46. For EC4, the test results are lower than the

predicted results, which are attributed to the fact that the B/t ratio exceeds the limitation. For GB50936, on the other hand, the B/t ratio of the specimens satisfies the limitation. Thus, the test results are very close to the predicted results. For AIJ and ACI318, the predictions are conservative, because the confining effect provided by the steel tube is not considered in the both design codes. In order to use the predictions of current design codes, the B/t ratio of RCFST column should satisfy the limitation of B/t ratio specified in the design code, so that the local buckling effect can be ignored in the strength-predictions. Otherwise, the strength reduction caused by local buckling should be considered.

5. Conclusions

This paper presents an experimental study on the axial compressive strength and ductility of RCFST stub columns with different spiral spacings and different concrete strengths. The following conclusions can be drawn within the scope of current studies:

- Compares with conventional CFST columns, the ultimate strength and ductility of the RCFST columns are increased due to the existing of the longitudinal reinforcing bars and spirals.
- Heavily arranged spirals (i.e., spiral spacing $s = 15$ mm) can considerably increase the ultimate strength. In the design of the spirally-confined RCFST columns, the requirements of the spiral spacing for the RC columns in Eq. (3) are also applicable for the RCFST columns.
- Spiral spacing has a considerable effect on increasing the ductility of RCFST columns. The ductility after the peak load increases considerably with decreasing the spiral spacing. Compared to conventional CFST columns, the ductility values DI improved by 39%, 72%, 103%, and 135% for specimens with spiral spacings of 45, 35, 25, and 15 mm, respectively.
- With increasing the concrete strength, the RCFST column ultimate strength increases while the ductility decreases. Spiral arrangement, even with a rather small spiral ratio, is an economical and easy solution for improving ductility of the RCFST columns with high strength concrete.
- The predicted strength of the composite columns from EC4 is slightly unsafe, while the prediction of AIJ and ACI 318 is conservative. Predictions from the GB50936 are the most precise. It is suggested that the confining effect of the steel tube on the concrete should be considered.

This paper examines the effect of the spiral spacing on the axial compressive behavior of RCFST columns with different concrete strengths. However, more test parameters, such as the steel tube strength, tube wall thickness, spiral strength, and column L/D ratio, are needed. Also, studies on the effect of spirals on seismic behavior of the RCFST columns are also needed to develop design criteria and construction measures.

Acknowledgments

This work was supported by a National Natural Science Foundation of China grant funded by the Chinese government (No. 51578020). Mou Ben is financially supported by first-class discipline project funded by the Education Department of Shandong Province. The support is greatly appreciated.

References

- ACI 318 (2014), Building Code Requirements for Structural Concrete and Commentary; American Concrete Institute, Farmington Hills, MI, USA.
- AIJ (2008), Recommendations for design and construction of concrete filled steel tubular structures; Architectural Institute of Japan, Tokyo, Japan.
- AISC (2016), Specification for Structural Steel Buildings; American Institution of Steel Construction, Chicago, IL, USA.
- Ding, F.X., Lu, D.R., Bai, Y., Zhou, Q.S., Ni, M., Yu, Z.W. and Jiang, G.S. (2016), "Comparative study of square stirrup-confined concrete-filled steel tubular stub columns under axial loading", *Thin-Wall. Struct.*, **98**, 443-453. <https://doi.org/10.1016/j.tws.2015.10.018>
- Eurocode 4 (2004), Design of Composite Steel and Concrete Structures; European Committee for Standardization, British Standards Institution, London, UK.
- GB 50010 (2010), Code for design of concrete structures; China Architecture & Building Press, Beijing, China.
- GB 50936 (2014), Technical code for concrete filled steel tubular structures; China Architecture & Building Press, Beijing, China.
- GB/T 50081 (2002), Standard for Method of Mechanical Properties on Ordinary Concrete; China Building Industry Press, Beijing, China.
- Hamidian, M.R., Jumaat, M.Z., Alengaram, U.J., Sulong, N.H.R. and Shafiq, P. (2016), "Pitch spacing effect on the axial compressive behaviour of spirally reinforced concrete-filled steel tube (SRCFT)", *Thin-Wall. Struct.*, **100**, 213-223. <https://doi.org/10.1016/j.tws.2015.12.011>
- Han, L.H. (2002), "Tests on stub columns of concrete-filled RHS sections", *J. Constr. Steel Res.*, **58**(3) 353-372. [https://doi.org/10.1016/S0143-974X\(01\)00059-1](https://doi.org/10.1016/S0143-974X(01)00059-1)
- Han, L.H., Ren, Q.X. and Li, W. (2010), "Tests on inclined, tapered and STS concrete-filled steel tubular (CFST) stub columns", *J. Constr. Steel Res.*, **66**(10), 1186-1195. <https://doi.org/10.1016/j.jcsr.2010.03.014>
- Hassan, M.M., Mahmoud, A.A. and Serror, M.H. (2016), "Behavior of concrete-filled double skin steel tube beam-columns", *Steel Compos. Struct. Int. J.*, **22**(5), 1141-1162. <https://doi.org/10.12989/scs.2016.22.5.1141>
- Huo, J.S., Huang, G.W. and Xiao, Y. (2009), "Effects of sustained axial load and cooling phase on post-fire behaviour of concrete-filled steel tubular stub columns", *J. Constr. Steel Res.*, **65**(8-9), 1664-1676. <https://doi.org/10.1016/j.jcsr.2009.04.022>
- Lee, H.J., Choi, I.R. and Park, H.G. (2017), "Eccentric compression strength of rectangular concrete-filled tubular columns using high-strength steel thin plates", *J. Struct. Eng.*, **143**(5), 1-11. [https://doi.org/10.1061/\(ASCE\)ST.1943-541X.0001724](https://doi.org/10.1061/(ASCE)ST.1943-541X.0001724)
- Liu, H.L. and Cai, J. (2013), "Research on behavior of rectangular CFST stub columns with binding bars under axial compression", *Proceedings of the 3rd International Conference on Civil Engineering, Architecture and Building*, Jinan, China, May.
- Krishan, A.L., Troshkina, E.A. and Astafyeva, M.A. (2017), "Strength of short concrete filled steel tube columns with spiral reinforcement", *Proceedings of the International Conference on Construction, Architecture and Technosphere Safety (ICCATS)*, Chelyabinsk, Russia, September.
- Marvel, L., Doty, N., Lindquist, W. and Hindi, R. (2014), "Axial behavior of high-strength concrete confined with multiple spirals", *Eng. Struct.*, **60**, 68-80. <https://doi.org/10.1016/j.engstruct.2013.12.019>
- Moon, J., Lehman, D.E., Roeder, C.W. and Lee, H.E. (2013), "Strength of Circular Concrete-Filled Tubes with and without Internal Reinforcement under Combined Loading", *J. Struct. Eng.*, **139**(12), 1-12. [https://doi.org/10.1061/\(ASCE\)ST.1943-541X.0000788](https://doi.org/10.1061/(ASCE)ST.1943-541X.0000788)
- Mou, B. and Bai, Y.T. (2018), "Experimental investigation on shear behavior of steel beam-to-CFST column connections with irregular panel zone", *Eng. Struct.*, **168**(08), 487-504. <https://doi.org/10.1016/j.engstruct.2018.04.029>
- Mou, B., Pang, L.Y., Qiao, Q.Y. and Yang Y.T. (2018), "Experimental investigation on unequal-depth-beam-to column joints with t-shape connector", *Eng. Struct.*, **174**(11), 663-674. <https://doi.org/10.1016/j.engstruct.2018.05.010>

- Nilson, A.H., Darwin, D. and Dolan, C.W. (2009), *Design of Concrete Structure*, McGraw Hill Education, New York, NY, USA.
- Pons, D., Espinos, A., Albero, V. and Romero, M.L. (2018), "Numerical study on axially loaded ultra-high strength concrete-filled dual steel columns", *Steel Compos. Struct., Int. J.*, **26**(6), 705-717. <https://doi.org/10.12989/scs.2018.26.6.705>
- Qiao, Q.Y., Zhang, W.W., Mou, B. and Cao, W.L. (2019), "Seismic behavior of exposed concrete filled steel tube column bases with embedded reinforcing bars: Experimental investigation", *Thin-Wall. Struct.*, **136**(3), 367-381. <https://doi.org/10.1016/j.tws.2018.12.039>
- Qu, X.S., Chen, Z.H. and Sun, G.J. (2015), "Axial behaviour of rectangular concrete-filled cold-formed steel tubular columns with different loading methods", *Steel Compos. Struct., Int. J.*, **18**(1), 71-90. <https://doi.org/10.12989/scs.2015.18.1.071>
- Ritchie, C.B., Packer, J.A., Seica, M.V. and Zhao, X.L. (2018), "Flexural behavior of concrete-filled double-skin tubes subject to blast loading", *J. Struct. Eng.*, **144**(7), 1-19. [https://doi.org/10.1061/\(ASCE\)ST.1943-541X.0002064](https://doi.org/10.1061/(ASCE)ST.1943-541X.0002064)
- Wei, H., Wang, H.J. and Hasegawa, A. (2014), "Experimental study on reinforced concrete filled circular steel tubular columns", *Steel Compos. Struct., Int. J.*, **17**(4), 517-533. <https://doi.org/10.12989/scs.2014.17.4.517>
- Xiamuxi, A. and Hasegawa, A. (2012), "A study on axial compressive behaviors of reinforced concrete filled tubular steel columns", *J. Constr. Steel Res.*, **76**, 144-154. <https://doi.org/10.1016/j.jcsr.2012.03.023>

BU